A Novel Voltage Controlled Crystal Oscillator (VCXO)

[1,2]Ulrich L. Rohde, *Fellow, IEEE*
[1]Univ. of Cottbus, BTU Cottbus 03046, Germany
[2]Synergy Microwave Corporation, NJ 07504, USA

Ajay K. Poddar, *Senior Member, IEEE*
Synergy Microwave Corporation, NJ 07504, USA
akpoddar@synergymwave.com

***Abstract*—The novel approach reported in this paper optimizes the start-up characteristics and drive sensitivity factor for achieving high performance voltage controlled crystal oscillator circuit (VCXO). An example of 100 MHz mode feedbacks and differential coupled VCXOs are demonstrated for the validation of this new approach, which allows fast start-up dynamics, including 8-12dB phase noise reduction, therefore, low noise, power-efficient and cost-effective solutions.**

I. Introduction

The phase noise is a critical figure-of-merit because it affects dynamic range, selectivity, and sensitivity of a receiver [1]-[37]. Recent analysis indicates that oscillator noise factor and crystal drive sensitivity influence phase noise significantly at relative closer to the carrier frequency [5]. Therefore, designing low cost high performance VCXO circuit is challenging for a given Q-factor, size, and power-consumptions. And, these objectives have been accomplished using empirical rules, therefore, predictive power of the VCXO model is limited [4]. This paper describes the methodology for realization of low cost high performance VCXOs solutions, even those with relative low Q-factor crystal resonators, for low phase noise and fast start-up VHF/UHF crystal oscillator applications.

II. Design Methodology

High frequency crystal resonator is a critical element for reference frequency standards in data communications. Low phase jitter of reference signal is a key factor to provide high quality processing. And, if we could establish the condition for frequency resonance modes at high VHF/UHF range by fundamental, we would be able to design the VHF/UHF VCXOs with excellent jitter characteristics without being influenced by the unwanted mode-jumping and spurious characteristics due to overtone modes characteristics.

A. Crystal Resonance Modes

The resonance frequency of the crystal is determined by the effective thickness of the quartz wafer, which is controlled by mechanical sawing and lapping of the quartz wafer to the desired thickness (*freq* $\propto$ *1/thickness)*. But there is a physical limit to the process and manufacture the thinner quartz wafer under the constraints of cost and reliability. Figure (1) shows the typical AT cut quartz crystal resonator and impedance characteristics for fundamental and overtone modes [37]. As shown in Figure (1), reducing wafer thickness beyond certain limit makes fragile and moreover, processing the component becomes more difficult as they get thinner. The conventional approach (without reducing the thickness of the quartz wafer) to obtain high frequency oscillation is to vibrate the crystal at odd order overtone modes of its fundamental frequency. Overtone modes (3^{rd}, 5^{th}, 7^{th}, 9^{th}, 11^{th}… 2n+1, where n is an integer) solution can translate frequency in VHF/UHF range but they are sensitive to spurious modes. And, as the overtone number goes up, the loss resistance R_i (Fig. 2b) of the crystal resonator increases by manifolds. Therefore, lowest overtone mode is preferred if that particular overtone number yields the desired higher resonance frequency.

Figure (2) shows the equivalent model and impedance characteristics of the quartz crystal, describes the multi-mode resonances. As shown in Fig. (2), the impedance magnitude of crystal exhibits strong resonances at the fundamental mode (f_0) and odd numbered overtones ($3f_0$, $5f_0$, and so on). Even numbered modes fail to exist due to insignificant resultant displacement of the electrodes, therefore, cannot be excited electrically. However, spurious resonance may be observed (Fig.1c) due to random vibrations in between fundamental (f_0) and odd overtone modes.

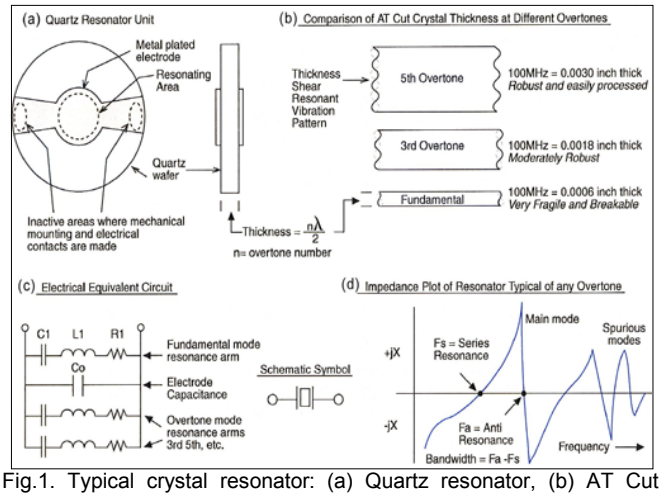

Fig.1. Typical crystal resonator: (a) Quartz resonator, (b) AT Cut crystal thickness at different overtones, (c) Equivalent circuit and (d) Impedance characteristics (fundamental & overtones) [37].

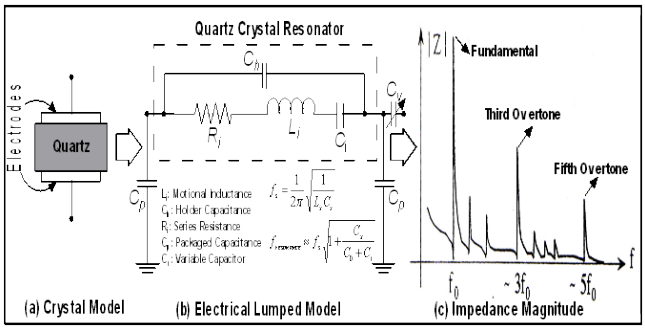

Fig.2. Typical crystal (a) Electrode model, (b) Electrical lumped model, and (c) Impedance characteristics (fundamental & overtones)

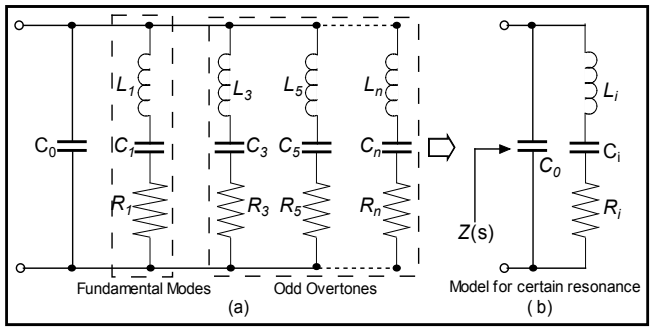

Fig.3. Typical distributed electrical equivalent circuit of a quartz crystal: (a) Includes all modes, (b) particular mode (*i*=1,3,5..*n*).

Figure (3) shows the typical electrical equivalent circuit of a quartz crystal that includes all the modes. Each series resonant circuit (R_i, L_i, C_i; i=1,3,5,7..) as shown in Figure (3a) represents a mechanical modes (excited by the piezoelectric effect), and the capacitor C_0 is the capacitance between the electrodes. In general, crystals are optimized with respect to a particular mode based on the design constraints and performance requirements suitable for typical VCXO topology. The first RLC branch (R_i, L_i, C_i) models the fundamental mode of oscillation, and the other branches are odd overtones, which are odd multiple of the fundamental frequency (Fig. 2). The overtone element values are calculated as $L_n = L$, $C_n = C/n^2$, $R_n = n^2R$; where n is the n^{th} overtone (n = 3, 5, 7…) [12, pp. 185].

The resistor R_i represents the heat dissipation due to mechanical friction in the crystal, L is the electrical equivalent of crystal mass, and the capacitor C represents the crystal stiffness or elasticity. The equivalent LCR circuit (Fig. 3b) described as motional arm of the crystal, and the shunt capacitor C_0 represents the static arm. The expression of the impedance for crystal resonator circuit (Fig. 3b) is given by

$$Z(s) = \frac{1}{sC_0 + \dfrac{1}{1/sC_i + sL_i + R_i}} = \frac{s^2 + sR_i/L_i + 1/L_iC_i}{sC_0[s^2 + sR_i/L_i + (C_0 + C_i)/L_iC_iC_0]} \quad (1)$$

$$Z(s) = \frac{s^2 + s\omega_0/Q + \omega_0^2}{sC_0\left\{s^2 + s\dfrac{\omega_0}{Q} + \omega_0^2\left[1 + \dfrac{C_i}{C_0}\right]\right\}} = \frac{(s - s_{z1})(s - s_{z2})}{C_0(s - s_{p0})(s - s_{p1})(s - s_{p2})} \quad (2)$$

$$s_{z1,2} = -\frac{\omega_0}{2Q} \pm j\omega_0\sqrt{1 - \frac{1}{4Q^2}} \approx -\frac{\omega_0}{2Q} \pm j\omega_0, \quad for \quad Q >> 1 \quad (3)$$

$$s_{p0} = 0, \quad s_{p1,2} = -\frac{\omega_0}{2Q} \pm j\omega_0\sqrt{1 + \frac{C_i}{C_0} - \frac{1}{4Q^2}} \quad (4)$$

Using $\left(\sqrt{1+x} \approx 1 + \dfrac{x}{2}, \; for \quad |x| < 1\right)$, (4) is approximated as

$$s_{p1,2} = -\frac{\omega_0}{2Q} \pm j\omega_0\sqrt{1 + \frac{C_i}{C_0} - \frac{1}{4Q^2}} \approx -\frac{\omega_0}{2Q} \pm j\omega_0\left(1 + \frac{C_i}{2C_0}\right) \quad (5)$$

$$Q = \frac{L_i\omega_0}{R_i} = \frac{1}{R_iC_i\omega_0} \quad (6)$$

where $s_{z1,2}$ and $s_{p1,2}$ are zero and poles, ω_0 is the series resonance frequency and Q is the quality factor.

From (3)-(5), series mode resonance of the crystal is represented by a small resistance in series with a resonant reactance, whereas, in parallel mode by a large resistor in parallel to a resonant susceptance. The series (f_i) and parallel resonance (f_p) are described by the impedance function (1), and can be evaluated from the imaginary part of the zeroes (3) and poles (5) as

$$\omega_i = \frac{1}{\sqrt{L_iC_i}} \Rightarrow f_i(series) = \frac{1}{2\pi\sqrt{L_iC_i}} \quad (7)$$

$$\omega_p \approx \omega_0\left(1 + \frac{C_i}{2C_0}\right)\Bigg|_{C_0 >> C_i} \Rightarrow f_p(parallel) \approx \frac{1}{2\pi\sqrt{L_iC_i}}\left(1 + \frac{C_i}{2C_0}\right)\Bigg|_{C_0 > C_i} \quad (8)$$

$$M = \frac{2Q(\omega_p - \omega_0)}{\omega_0} = \frac{2Q(f_p - f_0)}{f_0} \quad (9)$$

where M is mode separation (f_p - f_0). From (7), the degree to which an oscillator generates a constant frequency f_i throughout a specified period of time is defined as the frequency stability of the signal source.

B. Selection of The Desired Resonance Modes

Crystal resonator exhibits both desired and undesired modes therefore selection of the desired modes is critical for designing high frequency crystal oscillators. The fundamental frequency (lowest-mode) response is the most active due to lowest value of R_i (Fig. 3a). The resonance characteristic of the crystal resonator depends upon the thickness of the resonator. As the resonance frequency becomes higher, the thickness of crystal resonator becomes very thin and care must be taken to minimize the resonator drive level to avoid breakage of the resonator at high operating frequency.

To avoid the breakdown phenomena of the crystal resonator at high frequency, one can opt for higher series resistance of the crystal that will restrict the level of the current accepted and returned from the crystal but at the cost of increased noise resistance associated with the series resistance R_i (Fig. 2b). Higher order overtone mode (3rd, 5th, 7th, 9th, 11th… 2*n*+1, where *n* is an integer) will be active too but as the overtone number increases goes up, the loss resistance R_i (Fig. 3a) of the crystal inevitably increases. For high frequency operation, a method is needed to select a particular mode corresponding to desired frequency so that other active modes fail to sustained oscillations.

The novel approach is to maximize the negative resistance generated from the active device for a given mode and must yield positive value of resistance for all the other overtone modes including fundamental [37]. Figure (4) shows a typical Colpitts VCXO circuit for mode-selection analysis including noise contributions. The value of the input impedance Z_{in} (looking into the base of the transistor in Fig. 4) is [11]

$$Z_{in} \cong R_{in} + jX_{in} = -\left[\frac{Y_{21}}{\omega^2 C_1 C_2}\right]_{real} + \frac{1}{j\omega}\left[\frac{1}{C_1}+\frac{1}{C_2}\right]_{imaginary} \quad (10)$$

From (10), we notice that real part is negative (gain) and imaginary part is capacitive. The oscillator circuit shown in Figure (4) will oscillate if we select a crystal resonator that exhibits inductive property at fundamental mode and has lower value of loss resistance than the negative real part R_{in} generated by the active device network. Accordingly, crystal is selected, which can exhibit inductive motional reactance equals to capacitive reactance (X_{in}) of the network, and has a lower loss resistance than the negative real part R_{in} generated by the active circuit. The above arrangement of network will operate on the lowest available resistance mode associated with the crystal's fundamental mode resonance (lowest resonance frequency). For a higher frequency operation we have to operate on overtone mode, therefore reactive part (X_{in}) is to be dynamically controlled so that one of the feedback capacitor (C_1, C_2) can be made inductive to stop the oscillation at fundamental mode for a give frequency as

$$Z_{in} \cong R_{in} + jX_{in} = Y_{21}\left[\frac{L_2}{C_1}\right]_{real-part} + j\left[\omega L_2 - \frac{1}{\omega C_1}\right]_{imaginary-part} \quad (11)$$

From (11), we notice that even combined crystal and active device reactance conditions are satisfied, the positive real part conditions will not initiate oscillation under all conditions. Therefore, design goal is to create a condition where at the desired overtone mode crystal frequency, active device network has capacitance at both X_1 and X_2 position (effective negative resistance) and at the fundamental frequency, the active device network capacitance for one X value (X_1 or X_2) and inductor at the other (effective positive resistance). This condition can be achieved by incorporating tuning diode C_V and tuning the resonator network to a resonant frequency that lies between fundamental and overtone frequencies, therefore, network will have inductance for X_1 at the fundamental frequency and capacitance for X_1 at a given overtone frequency and only the target overtone resonance will have the potential to maintain stable oscillations. To validate the design approach, a 3rd overtone fast start-up 290 MHz VCXO is built as an example to apply the concept of mode-selection mechanism.

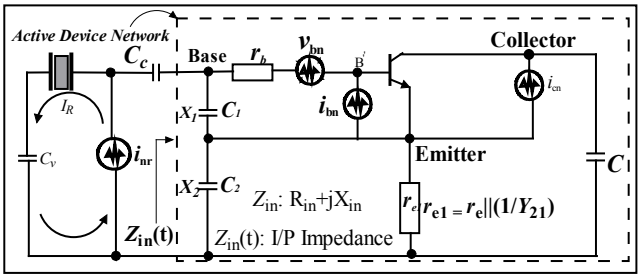

Fig.4. A typical Colpitts VCXO circuit including noise contributions

Figure (5) shows the schematic of the 3rd overtone 290 MHz VCXO in which fundamental and higher order overtone mode is (5th, 7th, 9th…$2n$+1, where n is an integer) is suppressed by mode-feedback and evanescent mode coupling techniques. This enables steep change of phases for pre-selected 3rd overtone mode, thereby maximization of group delay. However, the drawback of this approach is mode-jumping due to mode-feedback, which can be compensated by phase-shifter for suppressing of the unwanted oscillation. Figures (6) and (7) show the CAD simulated and measured phase noise plot (with and without mode-feedback). As shown in Figure (7), mode-feedback approach offers significant improvement in phase noise performances (-128 dBc/Hz @ 1kHz offset for 290 MHz carrier frequency).

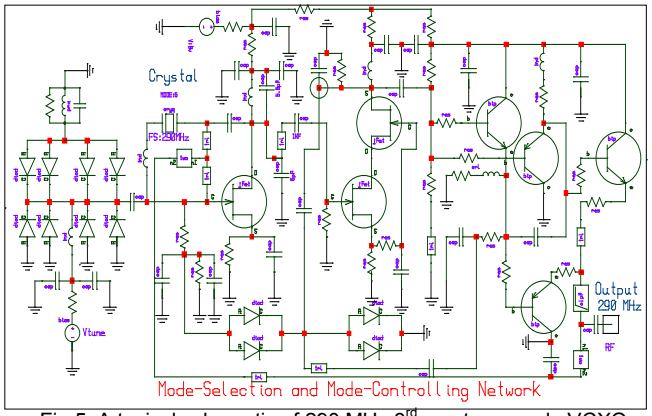

Fig.5. A typical schematic of 290 MHz 3rd overtone mode VCXO

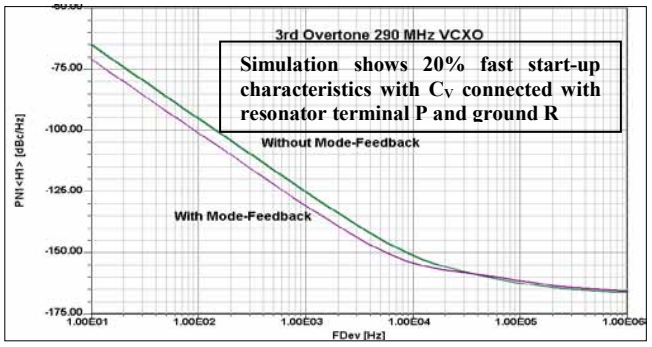

Fig.6. A CAD simulated phase noise plot of VCXO circuit (Fig. 5)

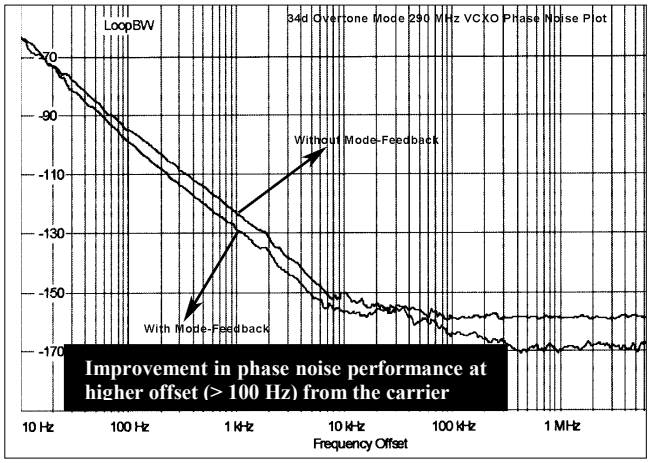

Fig.7. Measured phase noise plot 290 MHz 3rd overtone mode VCXO

At lower offset, we notice the deviation of 3-5dB between measured and simulated phase noise, the possible reason is inaccuracy of flicker parameters of crystal resonators and active device. The dynamic noise-feedback is an effective method to reduce the 1/*f* noise at lower offset (close-in).

III. START-UP, NOISE-FACTOR, DRIVE-LEVEL, PHASE-NOISE

As size of the communications equipment and portable electronic portable become smaller and smaller, crystal resonator size also shrinks to meet the real estate constraints. The reduction in crystal resonator size demands for larger activation current in the resonator network to enable fast oscillator start-up dynamics.

A. Oscillator Start-Up Characteristics And Drive Level

Oscillator start-up characteristics can be minimized by dynamically controlling the crystal drive-level, conduction angle, loop gain, Q-factor, loading, and noise Figure. In past, crystal oscillator used automatic gain control (AGC) to support low drive-level VCXO circuits. A typical VCXO with AGC consists of the oscillator stage, amplifier stage, and the rectifier stage. The output of the rectifier stage is fed back into the bias circuit to obtain steady-state oscillation at low drive-level. Due to large filter time constant in the rectifier stage, the start-up characteristics is very slow, therefore, AGC approach is not suited for portable telephone sets where frequent switch-on and switch-off of the power supply are repeated for the power saving of the batteries.

In addition to this, it is difficult to maintain low resonator drive level current I_R without reduction in the magnitude of the negative resistance $R_n(t)$ of conventional Colpitts crystal oscillator circuit (Fig. 8). From [11], negative resistance and resonator drive level at steady state can be described for circuit shown in Fig. (8) as

$$R_n = -\left[\frac{Y_{21}}{\omega^2 C_1 C_2}\right] \tag{12}$$

$$I_R \cong \frac{2I_E}{\omega C_2 R_n} \tag{13}$$

Where $$Y_{21}| = G_m(x) = \frac{qI_{dc}}{kTx}\left[\frac{2I_1(x)}{I_0(x)}\right]_{x=\frac{g_m I_R}{\omega C_1 I_E}} \tag{14}$$

$I_1(x)$ and $I_2(x)$ are the modified Bessel functions of order 0 and 1 respectively. From (12) and (13), resonator current drive level I_R can be lowered by increasing the value of feedback capacitor C_2 (Fig.8) for a given current I_E but at the cost of reduction in the value of negative resistance R_n.

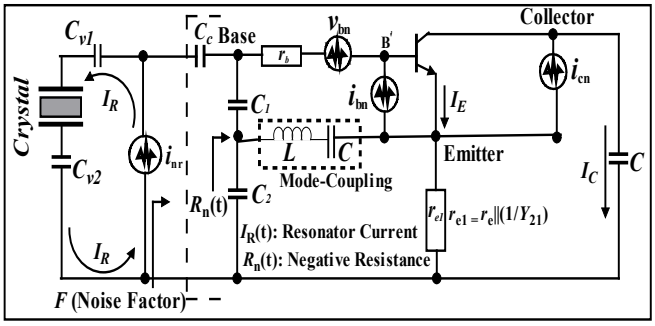

Fig.8. A typical Colpitts oscillator circuit including noise contributions

In order to maintain the same value of negative resistance R_n as required to compensate the loss resistance of the resonator at steady-state oscillation, the value of feedback capacitor C_1 (Fig.8) has to be reduced. But there is a practical limitation of the minimum value of the C_1 that is decided by a specified value of the load capacitance of the crystal resonator [33]-[36].

For high drive level, a non-linear effect, so-called amplitude-frequency effect, also interacts on the frequency value and degrades the 1/*f* noise performances in resonators [3]. Therefore, further reduction in the drive level will concentrate on the new proposed circuit using mode-coupling mechanism (tuning the L-C at higher overtone modes) and optimizing the ratio C_{V2}/C_{V1}) for improving the start-up characteristics and dynamic loaded Q at higher frequency (UHF/VHF). In general, coupling capacitor C_{V1} suffice the oscillation growth (without C_{V2}) but at the cost of slow start-up characteristics.

B. Oscillator Noise Factor (F) And Drive Level (y)

The expression for noise factor *F* and phase noise in dBc/Hz $\pounds(\omega)$ in terms of the oscillator feedback component (C_1 and C_2) for the circuit shown in Figure (8) can be described by [11, pp. 132, 180-181]

$$F = 1 + \frac{Y_{21}^+ C_2 C_c}{(C_1 + C_2)C_1}\left[r_b + \frac{1}{2r_e}\left(r_b + \frac{(C_1 + C_2)C_1}{Y_{21}^+ C_2 C_c}\right)^2\left(\frac{1}{\beta^+} + \frac{f^2}{f_T^2}\right) + \frac{r_e}{2}\right] \tag{15}$$

$$\pounds(\omega) = 10Log\left(\left(4kTR_L + \frac{4qI_c g_m^2 + \frac{K_f I_b^{AF}}{\omega} g_m^2}{\omega_0^2 C_1^2(\omega_0^2(\beta^+)^2 C_2^2 + g_m^2 \frac{C_2^2}{C_1^2})}\right)\left[\frac{\omega_0^2}{4\omega^2 V_{cc}^2}\right]\left[\frac{Q_u^2}{Q_L^2} + \frac{[C_1 + C_2]^2}{C_1^2 C_2^2 \omega_0^4 L^2 Q_L^2}\right]\right) \tag{16}$$

$$\beta^+ = \left[\frac{Y_{21}^+}{Y_{11}^+}\right]\left[\frac{C_1}{C_2}\right]^p; \quad g_m = \left[Y_{21}^+\right]\left[\frac{C_1}{C_2}\right]^q \tag{17}$$

where Y_{21}^+, Y_{11}^+ is the large signal [Y] parameter of the active device, K_f is the flicker noise coefficient, *AF* is the flicker noise exponent, R_L is the equivalent loss resistance of the tuned resonator circuit, I_c is the RF collector current, I_b is the RF base current, V_{cc} is the RF collector voltage, C_1, C_2 is the feedback capacitor (Fig. 8), Q_u and Q_L are unloaded and loaded Q factors, *p* and *q* are the drive level dependent constant across base-emitter of the device [4].

From curve-fitting attempts, the following values for *p* and *q* in (17) were determined (*p* =1.3 to 1.6; *q* =1 to 1.1). From (16), the expression of the phase noise is [11, pp. 181]

$$\pounds(\omega) = 10 \times \log\left[k_0 + \left(\frac{k^3 k_1 \left[\frac{Y_{21}^+}{Y_{11}^+}\right]^4 [y]^{4p}}{\left[Y_{21}^+\right]^6 [y]^{6q}}\right)\left(\frac{m^2(1+y)^2}{y^2(y^2+k)}\right)\right] \tag{18}$$

Where $k_0 = \frac{kTR}{\omega^2 \omega_0^2 L^2 V_{ce}^2 C_2^2}$, $k_1 = \frac{qI_{c0} g_m^2 + \frac{K_f I_b^{AF}}{4\omega} g_m^2}{\omega^2 \omega_0^2 L^2 V_{ce}^2}$,

$$k_2 = \omega_0^4 (\beta^+)^2, \quad k_3 = \omega_0^2 g_m^2, \quad k = \frac{k_3}{k_2 C_2^2} \quad and \quad m = \frac{Q_{unloaded}}{Q_{loaded}}$$

are constant for a given drive level with $y = \frac{C_1}{C_2}$. Differentiating (18) with respect to y will give condition for y_{opt} for optimum noise factor F_{opt} and minimum phase noise for a given bias and device parameters. From (15) and (16), feedback parameters (C_1 and C_2) are dynamically tuned for optimum noise factor F_{opt} for a given values of y_{opt} and β_{opt} which is dependent upon the drive level across base-emitter of the device [4]. Figure (9) shows the typical CAD simulated phase noise plot for a 100 MHz differential-Coupled crystal oscillator (Fig. 13) at offset 1 kHz from the carrier with respect to m_{opt}, F_{opt} and y_{opt}.

From (15) and (18), for different values of noise factor F ($F_3 > F_2 > F_1$), the phase noise can be lowest for m_{opt} =0.5 and y_{opt} = 2.2 (regime: 1.1 < y_{opt}< 3.2). It can be seen from Figure (9), for $F_{OPT} = F_1$(dB) = 6 dB, phase noise curve shows two minima for the values of $y_{1\ opt}$ =2.2 and $y_{3\ opt}$ =3.2, and one maxima corresponding to $y_{2\ opt}$ =1.1.

C. Crystal Resonator Frequency Drive Sensitivity

The dynamic coefficient of the crystal frequency-drive sensitivity in terms of the fractional change induced as a function of the square current can be described by [5]

$$k_d = \frac{f - f_0}{f_0 \times I^2} \Rightarrow f - f_0 = k_d \times f_0 \times I^2 \tag{19}$$

$$df = 2k_d \times f_0 \times I dI \Rightarrow \frac{df}{f_m} = \frac{2k_d \times f_0 \times I^2}{f_m} \times \frac{dI}{I} \tag{20}$$

where f_m is the modulation frequency, the spectral density of the oscillator output signal phase fluctuation $S_{\phi(f)}$ and amplitude fluctuation $S_{a(f)}$ can be described by [5]

$$S_{\phi(f)} = \left(\frac{\delta f}{f_m}\right)^2 = \delta\phi^2 \tag{21}$$

$$S_{a(f)}] = \left(\frac{\delta V}{V}\right)^2 = \left(\frac{\delta I}{I}\right)^2 \tag{22}$$

AM-to-PM conversion due to resonator drive level sensitivity can be given by 'γ' as

$$\gamma = \frac{S_{\phi(f)}}{S_{a(f)}} = \left(\frac{2k_d \times f_0 \times I^2}{f_m}\right)^2 = \left(\frac{2k_d \times f_0 \times P}{R_s \times f_m}\right)^2 \tag{23}$$

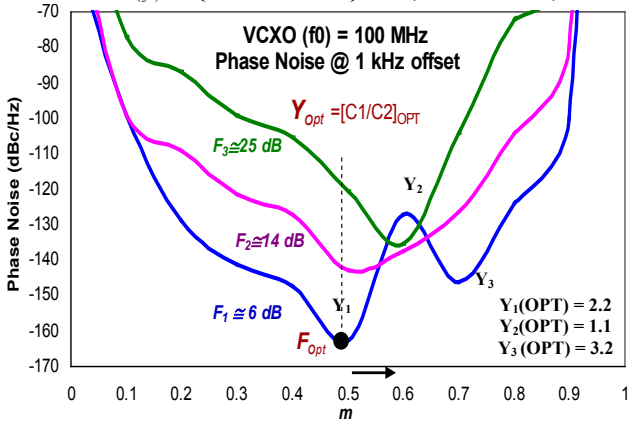

Fig. 9. Simulated phase noise plot of 100MHz XO (Fig. 13)

$$[S_{\phi(f)}]_{open-loop} = \frac{[S_{\phi(f)}]_{closed-loop}}{\left[1 + \left(f_0 / 2Q_L \times f\right)^2\right]} \tag{24}$$

where V is the voltage across the crystal resonator at series resonance, I is the current through the motional arm of the resonator (assuming the static capacitance is anti resonated), P is the power dissipated in the resonator ($P=I^2R_s$), R_s is the resonator series resistance, and Q_L is the resonator loaded Q factor. Figure (5) shows the typical oscillator phase noise plot for low and high resonator Q factor. For $f_0/(2Q_L f) >>1$, the value of k_d that results in the equal levels of oscillator closed PM noise level due to AM noise and open loop PM noise can be described by [5]

$$k_d^2 = \left[\frac{S_{\phi(f)}}{S_{a(f)}}\right]_{open-loop} \times \left[\frac{(10^3 \times R_s)^2}{(4 \times Q_L \times P)^2}\right] \tag{25}$$

For $f_0/(2Q_L f) >>1$, the value of k_d that results in the equal levels of oscillator closed PM noise level due to AM noise and open loop PM noise can be described by [5]

$$k_d^2 = \left[\frac{S_{\phi(f)}}{S_{a(f)}}\right]_{open-loop} \times \left[\frac{(10^3 \times R_s)^2}{(4 \times Q_L \times P)^2}\right] \tag{26}$$

From (25), k_d that would result in oscillator phase noise due to AM-FM conversion equal to the that due to the conversion of open loop PM noise to closed loop FM noise. For low phase noise applications, values of k_d has to be dynamically optimized by incorporating noise-filtering, noise-feedback, mode-feedback techniques.

D. Crystal Oscillator Phase Noise Reduction Techniques

There are mainly three noise sources that mostly contribute to the oscillator phase noise: shot noise, thermal noise, and flicker noise. Shot and thermal noise (broadband noise) generates amplitude and phase modulation of the carrier signal, resulting in equally divided amplitude modulation (AM) and phase modulation (PM) noise independent of frequency, and basically sets the noise floor of typical phase noise spectrum. The frequency flicker of an oscillator that appears as a $1/f^3$ slope in the phase noise spectral density originates from two basic phenomena: (1) $1/f$ phase noise turned into $1/f$ frequency noise via the Leeson effect, and (2) the $1/f$ fluctuation on the crystal resonator natural frequency [11, pp. 128].

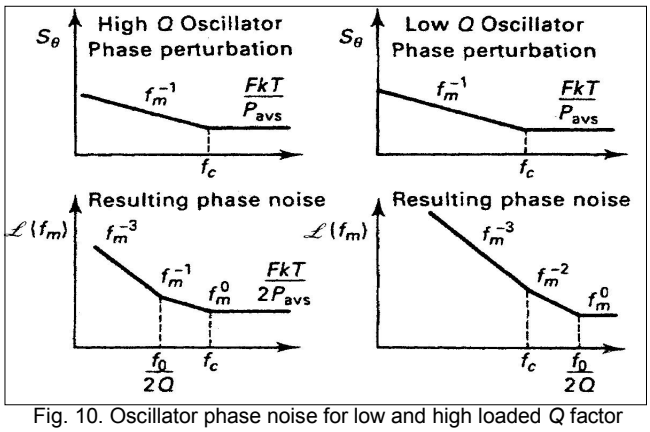

Fig. 10. Oscillator phase noise for low and high loaded Q factor

From (16), the modified Leeson equation by introducing tuning diode characteristics, appearing on pp. 332 in [11] is

$$\pounds(f_m) = 10\log\left\{\left[1+\frac{f_0^{\,2}}{[2f_mQ_0m(1-m)]^2}\right]\left(1+\frac{f_c}{f_m}\right)\frac{FkT}{2P_0}+\frac{2kTRK_0^2}{f_m^2}\right\} \quad (27)$$

where $\pounds(f_m)$, f_m, f_0, f_c, Q_L, Q_0, F, k, T, P_o, R, K_0 and m are the ratio of the sideband power in a 1Hz bandwidth at f_m to total power in dB, offset frequency, flicker corner frequency, loaded Q, unloaded Q, noise factor, Boltzman's constant, temperature in degree Kelvin, average output power, equivalent noise resistance of tuning diode, voltage gain and ratio of the loaded and unloaded Q. The expression of dynamic loaded Q is

$$Q_L = \frac{\omega_0}{2}\left[\frac{\partial\phi}{\partial\omega}\right] \quad (28)$$

$$\frac{\partial^n Q_L}{\partial\omega^n} = \frac{\omega_0}{2}\left[\frac{\partial^n\phi}{\partial\omega^n}\right]_{\omega=\omega_0,\phi=\phi_{opt}} \Rightarrow 0 \quad (29)$$

For maximum dynamic loaded Q, $\frac{\partial^n}{\partial\omega^n}[Q_L(\omega)]_{\omega=\omega_0} \to 0$, therefore, minimum phase noise can be found by differentiating (27) with respect to m, and equating to zero for minimum value of phase noise as

$$\frac{\partial^n}{\partial m^n}[\pounds(f_m)]_{m=m_{opt}} = 0 \Rightarrow (\phi = \phi_{opt})$$

$$\frac{d^n}{dm^n}\left[10\log\left\{\left[1+\frac{f_0^{\,2}}{[2f_mQ_0m(1-m)]^2}\right]\left(1+\frac{f_c}{f_m}\right)\frac{FkT}{2P_0}+\frac{2kTRK_0^2}{f_m^2}\right\}\right]_{m_{opt}} \quad (30)$$

$$m_{opt} \to 0.5 \Rightarrow \left[\frac{d^n\phi}{d\omega^n}\right]_{,\phi=\phi_{opt}} = \frac{Q_{unloaded}}{\omega_0} \text{ (Minimum noise)} \quad (30)$$

From (16) and (30), phase noise performance depends on the noise factor F of the oscillator circuit for a given Q factor, therefore, optimization of noise factor F with $m_{opt} = 0.5$ shall lead to improvement in phase noise performance.

IV. Examples And Validations

The new approach includes the mechanism to optimize the noise factor, start-up characteristics and resonator frequency drive sensitivity for high performance VCXO applications [22]-[29]. Figure (11) shows the practical example of 5th overtone 100 MHz VCXO circuit in which higher order mode is coupled through output path and feedback to the point where frequency-drive sensitivity of the crystal resonator shows maximum group delay and faster slew rate, resulting, improved phase noise performance.

As shown in Figure (12), mode-feedback approach minimizes the phase noise by 10-12dB, and the typical measured phase noise is -138 dBc/Hz @ 100 Hz for a given crystal resonator Q factor of ~ 2×10^6. At lower offset (10 Hz), improvement in phase noise performance is limited due to the influence of crystal 1/*f* noise, which can be minimized by dynamically optimizing the crystal resonator frequency drive sensitivity factor. The dynamic optimization of resonator frequency drive sensitivity is an effective method to reduce the 1/*f* noise of high Q crystal resonator based oscillators.

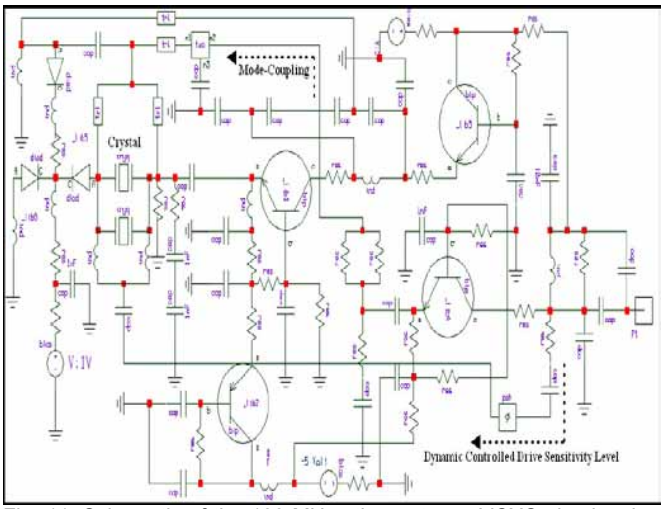

Fig. 11. Schematic of the 100 MHz 5th overtones VCXO circuit using high quality factor crystal resonator (Q≅2E6)

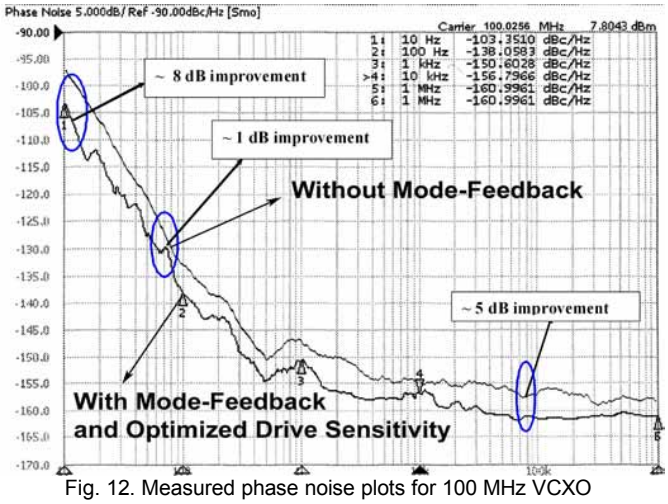

Fig. 12. Measured phase noise plots for 100 MHz VCXO

In addition to this, the differential coupled mode-feedback approach (13) discussed in this work includes a methodology for optimum coupling to enhance the dynamic loaded Q, and to reduce or eliminate phase hits, while reducing the thermal drift and susceptibility to microphonic to an extremely low level, and retaining low phase noise and broadband tunability. As shown in Fig. (13), the mode-feedback and differential coupled push-pull noise dynamics is optimized for minimum phase noise for low Q resonator (Q ≅ 60,000).

Figure (14) shows the plots of differential coupled 100 MHz crystal oscillator (XO) for comparative phase noise analysis and validation of the mode-feedback and noise-filtering approach for a given values of F_{opt}, y_{opt}, β_{opt} and m_{opt} as discoed in section (III). Figure (13) incorporates the component values as per above design calculations (as discussed in Section III). Figure (14) shows the CAD simulated phase noise plots for conventional Colpitts VCXO and this work (Noise-Feedback, Mode-Feedback and Mode-Feedback & Noise Filtering) for a typical 100 MHz crystal oscillator circuits. Figure (15) shows the measured phase noise plot, which closely agree with the simulated result for both approaches (with and without mode-feedback).

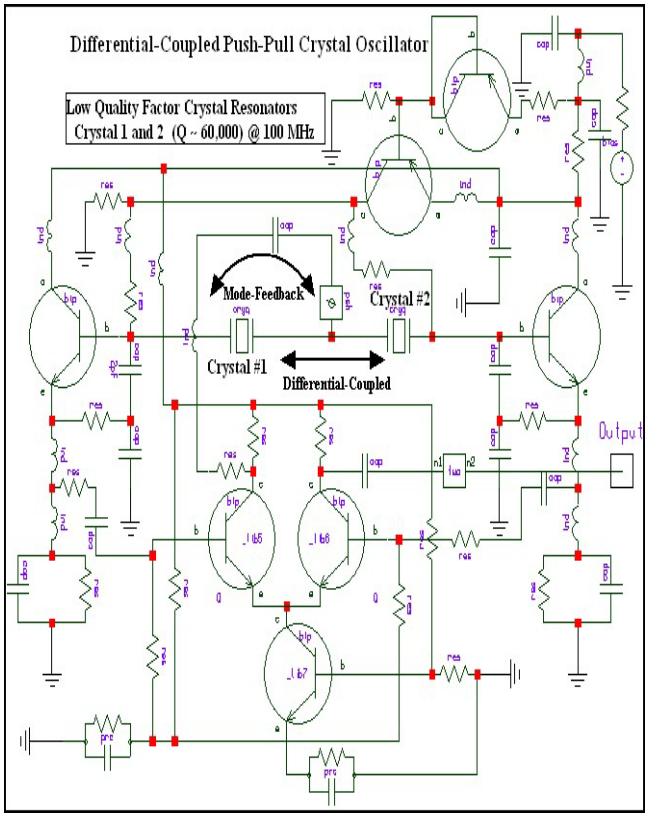

Fig. 13. Schematic of 100 MHz differential-coupled push-pull crystal oscillator Circuit using inexpensive crystal resonators (Q ≅ 60,000)

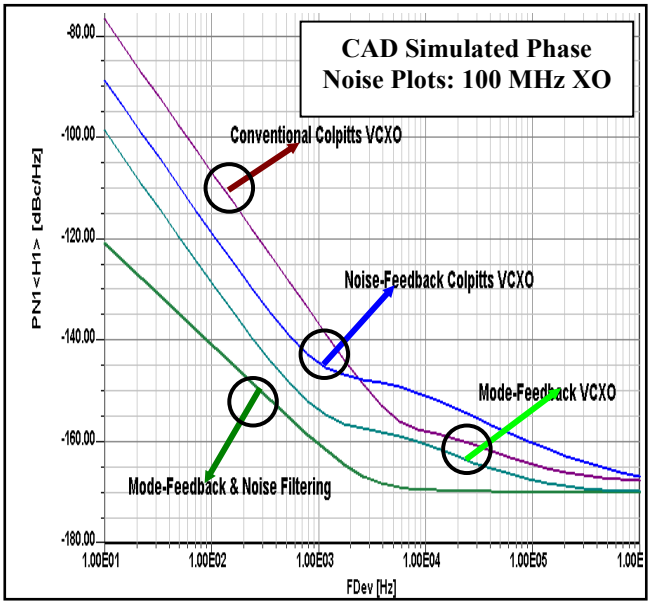

Fig. 14. Simulated phase noise plots for 100 MHz XO

At lower offset (<10 Hz), improvement in phase noise performance is limited due to the influence 1/*f* noise, which can be optimized by selecting transistor that has low value of 1/*f* noise. The typical measured phase noise is –141 dBc/Hz at 100 Hz offset from the carrier (using inexpensive crystal resonator with a quality factor of ~ 60,000), and to author knowledge this is the reasonably low phase noise solution for this class of inexpensive crystal oscillators.

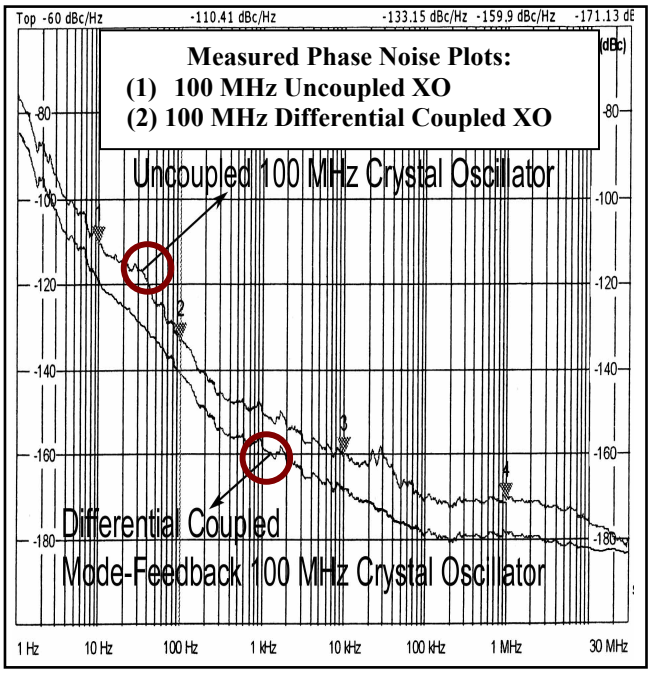

Fig. 15. Measured phase noise plots for 100 MHz differential XO

V. Conclusions

This work offers cost-effective solution and can be applied for a crystal resonator (both high-Q and low-Q) based VCXOs for substantial reduction in phase noise. The reported techniques optimize the drives sensitivity and noise factor for achieving low cost and low phase noise crystal oscillator circuits. Competing other alternative semiconductor technologies may not deliver the same level performance in terms of cost, size, and power.

References

[1] E. Rubiola and V. Giordano, " On the 1/*f* Frequency Noise in Ultra-Stable Quartz Oscillators", 2006 IEEE FCS.

[2] D. B. Leeson, "A Simple Model of Feedback Oscillator Noise Spectrum, " *IEEE, Proc.* pp. 329-332, 1966.

[3] S. Galliou, F. Sthal, and M. Mourey, " Enhanced Phase Noise Model For Quartz Crystal Oscillators", 2002 IEEE FCS.

[4] U. L. Rohde and A. K. Poddar, "Noise Minimization Techniques for RF & MW Signal Sources (Oscillators/VCOs)", MW Journal, Sept. 2007.

[5] M. M. Driscoll, "Oscillator AM-to-FM Noise Conversion Due to the Dynamic Frequency- Drive Sensitivity of the Crystal Resonator", 2008 IEEE Frequency Control Symposium FCS, pp. 672-676.

[6] S. Galliou, F. Sthal, N. Gufflet, and M. Mourey," Predicting Phase Noise in Crystal Oscillators", IEEE FCS 2002.

[7] M. M. Driscoll, "Low Noise, VHF Crystal-Controlled Oscillator Utilizing Dual, SC-Cut Resonators", IEEE Tran. on UFFC, Vol. UFFC-33, No. 6, pp. 698-704, Nov. 1986.

[8] W-Thai Hsu," Resonator Miniaturization for Oscillators", 2008 IEEE Int'l Frequency Control Symposium, pp. 392-395.

[9] G. Ernst et. al., "Reducing Phase Noise Degradation Due to Mechanical Vibration on High Performance Quartz Resonator Osc. for Gateway Applications", 2008 IEEE FCS.

[10] U. L. Rohde and A. K. Poddar, "*Feedback and Mode-Coupling Improves The Phase Noise Performances of The Crystal Oscillators*" 2008 IEEE FCS, pp. 554-561.

[11] U.L. Rohde, A.K. Poddar, and G. Boeck, *The Design of Modern Microwave Oscillators for Wireless Applications: Theory and Optimization*, Wiley, New York, 2005.

[12] G. Gonzalez, *Foundations of Oscillator Circuit*, Ch-IV, 2007 Artech House, Inc., London.

[13] U. L. Rohde and A. K. Poddar, "Dynamic Noise-*Feedback and Mode-Coupling Mechanism Silences The VCXOs Phase Noise*" 2008 IEEE Int'l FCS, 18-21 May 2008, Hawaii, USA.

[14] Y. S. Shmaliy, "One-Port Noise Model of a Crystal Oscillator", *IEEE Trans.* on *U, F* and *FCS*, Vol. 51, No. 1, Jan. 2004.

[15] D. V. Bogomolov, R. Boroditsky, " Low Phase Noise UHF TCXO", Proc. Of the 2005 *IEEE IFCS*, pp. 509-511, 2005.

[16] X. Huang, W. W, Feng Tan, and W. Fu, " High-Frequency Overtone TCXO Based on Mixing of Dual Crystal Oscillators", *IEEE Trans.* on *U, F,* and *FC,* Vol. 54, No. 6, pp. 1103-1107, June 2007.

[17] M. E. Frerking, Fifty years of progress in quartz crystal frequency standards, " in Proc. IEEE Int. Freq. Contr. Symp., 1996, pp. 33-46.

[18] M. Q. Li, X. H. Huang, F. Tan, Y.-H. Fan, and X. Liang, " A novel microcomputer temperature-compensating method for an overtone crystal oscillator," IEEE Trans. Ultrasonic, Ferroelectric, Frequency Control, vol., 52, no. 11, pp. 1919-1922, Nov. 2005.

[18] E. Jackson, H. Phillips, and B. E. Rose, " The microcomputer compensated crystal oscillator a progress report, " in Proc. IEEE Int. Freq. Contr. Symp., 1996, pp. 687-692.

[19] K. Hennessy, "Quartz Crystal Basics: From Raw Materials to Oscillators", High Frequency Electronics, pp. 54-58, Dec. 2007.

[20] J. R. Westra, C. J. M. Verhoeven, A. H. M. Van Roermund, " Resonance-mode selection and cross talk elimination using resonator-synchronized relaxation oscillators", Solid-State Circuits Conference, 1988, ESSCIRC apos: 98, pp. 88-91, Sept 1998.

[21] F. Sthal, S. Galliou, N. Gufflet, and M. Mourey, " Predicting Phase Noise in Crystal Oscillators", *IEEE Trans.* on *U, F,* and *FC,* Vol. 52, No. 1, pp. 27-30, June 2005.

[22] U. L. Rohde and A. K. Poddar, "Wideband voltage controlled oscillators employing evanescent mode coupled resonators," *US Patent No*. 71803812, Feb 2007.

[23] U. L. Rohde and A. K. Poddar," Integrated Low Noise Microwave Wideband Push- Push VCO", *US Patent No*. 7,088189, Aug 2006.

[24] U. L. Rohde and A. K. Poddar," User-Definable Thermal Drift Voltage Controlled Oscillator", US Patent No.7, 265,642 B2, Sept 4, 2007.

[25] U. L. Rohde and A. K. Poddar," Low Thermal Drift Tunable Frequency Voltage Controlled Oscillatory", US Patent No.7262670 B2, Aug 2007.

[26] U. L. Rohde and A. K. Poddar," Tunable Oscillator", US Patent No.7, 292,113, Nov. 6, 2007.

[27] U. L. Rohde and A. K. Poddar," Tunable Frequency, Low Phase Noise and Low Thermal Drift Oscillator", *US Patent No.7196591*, 2007.

[28] U. L. Rohde and A. K. Poddar," Multi-Octave Band Tunable Coupled-Resonator Oscillator", *US Patent No.* 292,113, Nov. 6, 2007.

[29] U. L. Rohde and A. K. Poddar," Low Noise, Hybrid Tuned Wideband Voltage Controlled Oscillator", *US Patent No.* 7,365,612, April 2008.

[30] A. Grebennikov, RF and Microwave Transistor Oscillator Design, John Wiley & Sons Ltd., 2007, UK.

[31] J.K.A. Everard and C. Broomfield, "Reduced Transposed Flicker Noise in Microwave Oscillators using GaAs based Feedforward Amplifiers", IEEE Transactions on Ultrasonics Ferroelectrics and Frequency Control. Vol. 54, No. 6, June 2007, pp.1108 – 1117

[32] Randall W. Rhea, *Oscillator Design And Computer Simulation,* 2nd ed., SciTech Publishing, Raleigh, NV, 2006.

[33] Y Tsuzuki, T. Adachi, and J. W. Zhang, " Fast Start-up Crystal Oscillator Circuits", 1995 IEEE International Frequency Control Symposium Digest, pp. 565-568.

[34] Y Tsuzuki, T. Adachi, and J. W. Zhang, " Formulation of Nonlinear Negative Resistance For Calculation of Start-up Characteristics of Crystal Oscillatorstor Circuits", 1996 IEEE International Frequency Control Symposium Digest, pp. 710-713.

[35] Y Tsuzuki, T. Adachi, and H. Yokohara, " Low Drive Level Crystal Oscillator Circuit", 1997 IEEE International Frequency Control Symposium Digest, pp. 966-969.

[36] Yu. S. Shmaliy, A. V. Marienko, O. Ibarra-Manzano, and R. Rojas-Laguna," Flicker Noise Conversion in Crystal Oscillator", Proc. Of the 2002 IEEE International Frequency Control Symposium and PDA Exhibition, pp. 665-672

[37] D. Nehring, "Novel high-frequency crystal oscillator cuts jitter and noise", RF Design Journals, pp. 32-42, June 2005.